catalysts

MDPI

Article

The Influence of Sulfurization and Carbonization on Mo-Based Catalysts for CH_3SH Synthesis

Hao Wang [1,2], Wenjun Zhang [1,3,*], Dalong Zheng [1,2,*], Yubei Li [1,4], Jian Fang [1,4], Min Luo [1,4], Jichang Lu [1,4] and Yongming Luo [1,4]

1 Faculty of Environmental Science and Engineering, Kunming University of Science and Technology, Kunming 650500, China; 20212207125@stu.kust.edu.cn (H.W.); lyb_0134@163.com (Y.L.); fj202102@163.com (J.F.); rengkeluo@163.com (M.L.); lujichangc7@kust.edu.cn (J.L.); environcatalysis@kust.edu.cn (Y.L.)
2 Zibo Vocational Institute, Zibo 255300, China
3 Yunnan Provincial Department of Ecology and Environment in Lijiang City Ecological Environment Monitoring Station, Lijiang 674100, China
4 The Innovation Team for Volatile Organic Compounds Pollutants Control and Resource Utilization of Yunnan Province, The Higher Educational Key Laboratory for Odorous Volatile Organic Compounds Pollutants Control of Yunnan Province, Kunming 650500, China
* Correspondence: zhangwenjun202109@126.com (W.Z.); 12648@zbvc.edu.cn (D.Z.); Tel./Fax: +86-87-165103845 (W.Z.)

Abstract: Sulfur-resistant Mo-based catalysts have become promising for the one-step synthesis of methanethiol (CH_3SH) from $CO/H_2/H_2S$, but the low reactant conversion and poor product selectivity have constrained its development. Herein, we synthesized K-MoS_2/Al_2O_3 and K-Mo_2C/Al_2O_3 catalysts via the sulfurization and carbonization of K-Mo-based catalysts in the oxidized state, respectively. During the synthesis of CH_3SH, both K-Mo_2C/Al_2O_3 and K-MoS_2/Al_2O_3 showed excellent catalytic performance, and the activity of the former is superior to that of the latter. The effect of different treatments on the catalytic performance of Mo-based catalysts was investigated by XRD, BET, Raman spectroscopy, H_2-TPR, and reactants-TPD characterization. The results showed that the sulfide-treated sample showed stronger metal-support interactions and contributed to the formation of K_2S, which exposed more active sites and stabilized the formation of C-S bonds. Carbonized samples enhanced the activation of H_2, which promoted the hydrogenation of the intermediate species of carbonyl sulfide (COS) and thus improved the selectivity of CH_3SH.

Keywords: Mo_2C; MoS_2; CH_3SH synthesis; $CO/H_2/H_2S$-TPD

check for updates

Citation: Wang, H.; Zhang, W.; Zheng, D.; Li, Y.; Fang, J.; Luo, M.; Lu, J.; Luo, Y. The Influence of Sulfurization and Carbonization on Mo-Based Catalysts for CH_3SH Synthesis. *Catalysts* **2024**, *14*, 190. https://doi.org/10.3390/catal14030190

Academic Editor: Valeria La Parola

Received: 13 November 2023
Revised: 1 December 2023
Accepted: 14 December 2023
Published: 11 March 2024

1. Introduction

The extensive use of coal, particularly coal gasification, has caused serious air pollution, such as CO, and reduced sulfur species (e.g., H_2S, COS, and CS_2), of which H_2S dominates [1]. Excessive emissions of these pollutants may worsen harmful environmental pollution (haze and acid rain) [2,3]. Due to the significant differences in the physicochemical properties of H_2S and CO, they typically require different removal strategies. Common methods for removing H_2S include catalytic hydrogenation [4], hydrolysis [5], and the Claus process [6]. However, most of the final products are converted to low-value solid sulfur or secondary pollutants, and the sulfur-containing species often poison the catalysts. CO is mainly treated using catalytic oxidation technologies [7,8], which wastes resources and consumes excessive energy. Therefore, a meaningful strategy would be the synergistic removal and resource utilization of CO and H_2S.

CH_3SH is an important precursor of methionine, an essential amino acid for poultry and animal feed [9]. Methionine also has applications in the fields of medicine, food, biology, and cosmetics and can be used as a moderator for free-radical polymerization to produce pesticides [10]. The thiolation of methanol is the main method for synthesizing

methyl mercaptan in the industry [11,12], in which methanol can be synthesized by syngas ($CO + H_2$). To reduce the costs of synthesizing CH_3SH, H_2S produced during coal gasification and syngas ($CO + H_2$) can be directly utilized as a feedstock for the one-step synthesis of CH_3SH [13]. Theoretically, the product of the one-step synthesis of CH_3SH from $CO/H_2/H_2S$ contains only CH_3SH and H_2O (Equation (1)) and thus provides a clean and economical synthetic route. However, the conversion of CO and the selectivity of CH_3SH are usually unsatisfactory in practice. Therefore, the development of high-performance catalysts for the synthesis of CH_3SH has received increasing attention.

Molybdenum disulfide (MoS_2) is widely used during hydrodesulfurization, low-carbon mixed-alcohol synthesis, mercaptan synthesis, etc. [10,14], due to its unique two-dimensional layered structure and semiconducting properties. MoS_2 is bonded by strong S-Mo-S bonds within layers and weak van der Waals forces between layers, and the addition of alkali metals can modulate the electronic effect on the Mo surface [15,16]. Therefore, molybdenum sulfide-based catalysts have become the main catalysts used in methanethiol synthesis due to their high sulfur resistance and stability [17–19]. In the past decades, the catalytic synthesis of CH_3SH in a mixed $CO/H_2/H_2S$ gas system over K-Mo-based catalysts has been investigated in terms of gas components, support properties, additive type, calcination temperature and atmosphere, and preparation method. The nature of the support greatly influences the metal-support interactions as well as the dispersion of the active metal [20]. Stronger metal-support interactions can promote interfacial charge transfer, change the metal structure, and modulate molecular adsorption [21,22]. In addition, the dispersion of active metals can expose more active sites and accelerate the reaction [2]. However, there are still some acute problems limiting the practical applications of MoS_2 during the synthesis of CH_3SH, such as its low selectivity and poor stability.

In recent years, molybdenum carbide (Mo_2C) has received attention as a catalyst due to its high melting point, high hardness, high tensile strength, and high electrical and thermal conductivity, which are similar to ceramics [23–25]. Mo_2C is an intercalation compound formed by the entry of carbon atoms into the interstices of molybdenum atoms. The structure of molybdenum carbide is determined by a combination of geometrical and electronic factors. Carbon atoms that enter between molybdenum atoms occupy metal sites in the precursor, which changes the structure. Typically, crystals have face-centered cubic (fcc), hexagonal closed-packed (hcp), and simple hexagonal (hex) structures. Scholars believe that three types of bonding between atoms exist in Mo_2C: (i) metallic bonding (rearrangement of metal–metal bonds); (ii) covalent bonding (formation of bonds between metals and carbon); (iii) ionic bonding (charge transfer between metals and carbon) [26]. Mo_2C also possesses strong sulfur resistance and hydrogen evolution capacity, allowing it to be applied during CH_3SH synthesis. However, there have been no reports on the utilization of Mo_2C-based catalysts for synthesizing CH_3SH in $CO/H_2/H_2S$ mixtures. Therefore, there is a need to compare the catalytic performance and physicochemical properties of K-Mo-based catalysts treated via sulfidation and carbonization to help guide the design of efficient Mo-based catalysts.

In this work, we first modulated the support and reaction pressure to determine the optimal reaction conditions to synthesize CH_3SH from $CO/H_2/H_2S$. Then, K-MoS_2/Al_2O_3 and K-Mo_2C/Al_2O_3 catalysts were synthesized by sulfidation and carbonization treatments, respectively. This was performed to understand the effects of different treatments on their physicochemical properties and catalytic behaviors. Both catalysts showed excellent catalytic activity. BET, XRD, Raman spectroscopy, H_2-TPR, and reactants-TPD were used to characterize K-MoS_2/Al_2O_3 and K-Mo_2C/Al_2O_3 catalysts. The results revealed that the key reason for the high performance of K-MoS_2/Al_2O_3 was its strong metal-support interactions, while the performance of K-Mo_2C/Al_2O_3 was attributed to its ability to activate H_2. This work provides new ideas for the modification of Mo-based catalysts applied to CH_3SH synthesis.

2. Results and Discussion

2.1. Effect of Reaction Pressure and Support

Figure 1 shows the CO conversion and product selectivity over K-MoS_2/SiO_2 and K-MoS_2/Al_2O_3 catalysts during the synthesis of CH_3SH from CO/H_2/H_2S. The effect of reaction pressure on the synthesis of CH_3SH was investigated in terms of the catalysts' activity. As shown in Figure 1a, the CO conversion remained at about 5% and hardly changed upon increasing the temperature at a reaction pressure of 0 MPa. When the reaction pressure was increased to 0.2 MPa, the CO conversion significantly increased and further increased with the temperature, indicating that pressure directly affected the CO conversion. Figure 1b,c show the selectivity of the products under different pressures. When the reaction system was unpressurized, the main products were COS, CS_2, and CH_3SH, among which COS was the main product and showed the highest selectivity (~60%). The selectivity of CH_3SH was unsatisfactory. When the reaction system was pressurized to 0.2 MPa, CH_3SH was the main product, which had a maximum selectivity of 62.5% at 325 °C, accompanied by the generation of some COS and CO_2. When the pressure in the system increased, the hydrogenation of the intermediate product COS to generate CH_3SH was accelerated, while the hydrolysis of COS to CO_2 was promoted, and the decomposition of CH_3SH into CS_2 was inhibited. It can be seen that the synthesis of CH_3SH from CO/H_2/H_2S was greatly promoted by pressurizing the reaction system, and side reactions were also inhibited, which promoted the generation of CH_3SH.

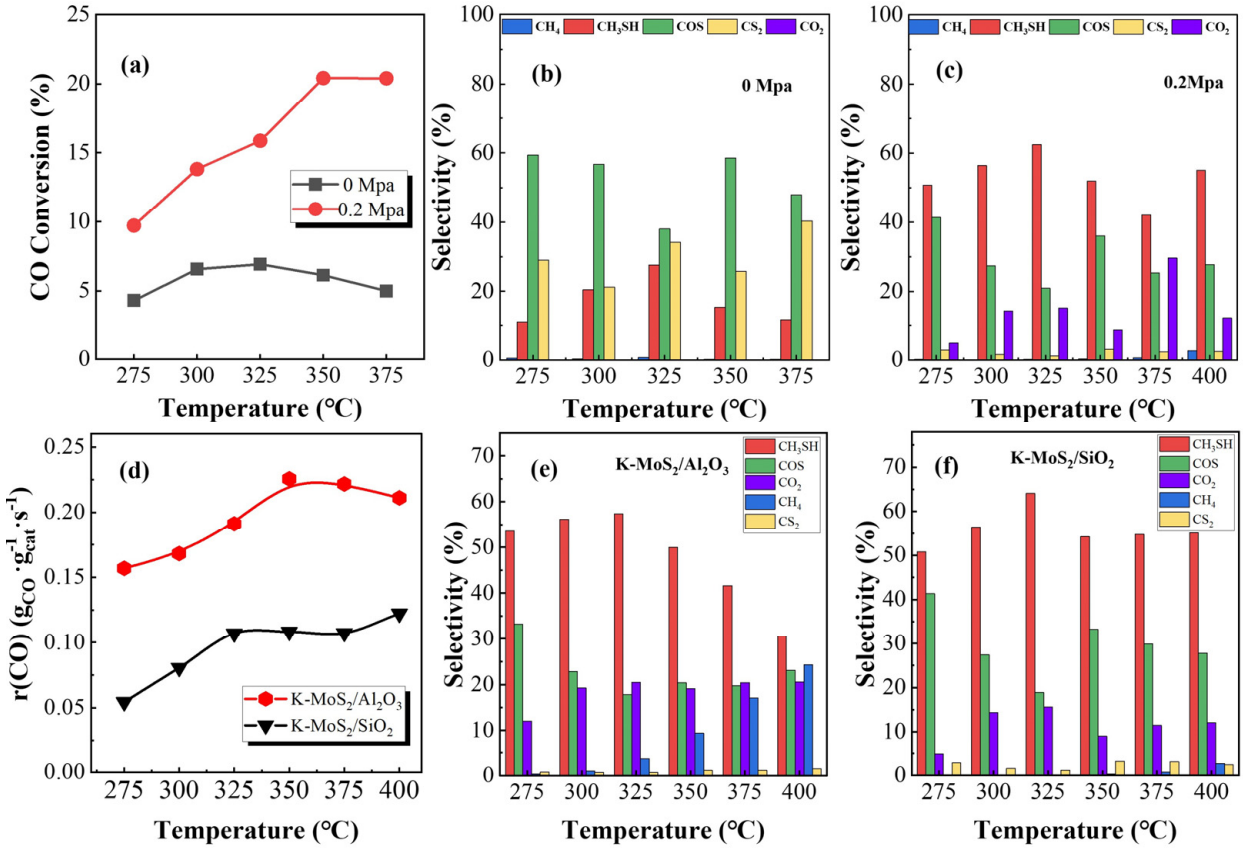

Figure 1. (**a**) CO conversion over K-MoS_2/Al_2O_3 at 0 MPa and 0.2 MPa. Product selectivity over K-MoS_2/Al_2O_3 catalyst at 0 MPa (**b**) and 0.2 MPa (**c**); (**d**) consumption rate of CO at 0.2 MPa over K-MoS_2/Al_2O_3 and K-MoS_2/SiO_2. Product selectivity over K-MoS_2/Al_2O_3 (**e**); K-MoS_2/SiO_2 (**f**).

The sulfided K-Mo catalysts with different supports were compared during the synthesis of CH_3SH from CO/H_2/H_2S at 0.2MPa. As shown in Figure 1d, the CO consumption rate was higher over the K-MoS_2/Al_2O_3 catalyst, which was almost three times that of K-MoS_2/SiO_2. K-MoS_2/Al_2O_3 showed the highest consumption rate of CO at 350 °C, ex-

ceeding 0.23 g(CO)·g^{-1}(cat)·h^{-1}. In Figure 1e,f, the products obtained over K-MoS_2/SiO_2 and K-MoS_2/Al_2O_3 catalysts both mainly consisted of CH_3SH, COS, CO_2, CH_4, and CS_2, among which there was no significant difference in the selectivity of CH_3SH. However, K-MoS_2/Al_2O_3 possessed a higher CH_4 selectivity at high temperatures due to the over-hydrogenation of CH_3SH, while K-MoS_2/SiO_2 had a weaker hydrogenation ability, resulting in a higher COS selectivity. In summary, K-MoS_2/Al_2O_3 using Al_2O_3 as the support under pressurized conditions was more favorable for the synthesis of CH_3SH from CO/H_2/H_2S.

2.2. Performance of the Sulfided and Carbonized Catalysts

2.2.1. Characterization of the Phase Structure

The N_2 adsorption–desorption of K-MoS_2/Al_2O_3 and K-Mo_2C/Al_2O_3 catalysts was characterized to further elucidate the differences in their physical properties. The corresponding isotherms are shown in Figure 2a, and the detailed information is shown in Table 1. The isotherms of K-MoS_2/Al_2O_3 and K-Mo_2C/Al_2O_3 were assigned as type-IV with H-1type hysteresis loops, indicating mesoporous structures [27–29]. In contrast, the BET surface area of K-Mo_2C/Al_2O_3 was larger than that of K-MoS_2/Al_2O_3, possibly due to the accumulation of sulfur on the surface of K-MoS_2/Al_2O_3 due to vulcanization, whereas the carbonization treatment avoided this.

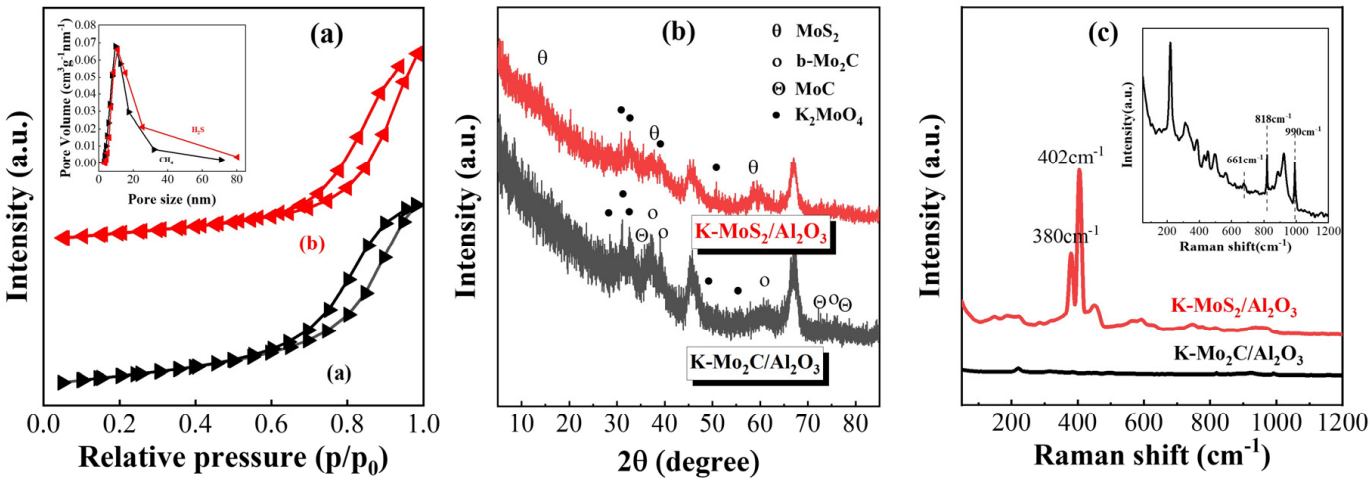

Figure 2. N_2 adsorption–desorption isotherms (**a**), XRD patterns (**b**), and Raman spectra (**c**) of K-MoS_2/Al_2O_3 and K-Mo_2C/Al_2O_3 samples.

Table 1. Physical properties of K-Mo_2C/Al_2O_3 and K-MoS_2/Al_2O_3.

Sample	Surface Area (m^2/g)	Pore Volume (cc/g)	Pore Diameter Dv (*d*) (nm)
K-Mo_2C/Al_2O_3	103.9	0.321	9.618
K-MoS_2/Al_2O_3	82.2	0.326	8.615

X-ray diffraction (XRD) was used to reveal the crystalline phases of K-MoS_2/Al_2O_3 and K-Mo_2C/Al_2O_3 catalysts, and the corresponding XRD patterns are shown in Figure 2b. Diffraction peaks (2θ = 38.1, 39.4, 61.7, and 75.7°) corresponding to the (002), (101), (110), and (201) planes of β-Mo_2C (JCPDS#65-8766) were observed in the pattern of K-Mo_2C/Al_2O_3. Moreover, K-Mo_2C/Al_2O_3 also displayed weak characteristic diffraction peaks attributed to MoC (JCPDS#08-0384). For K-MoS_2/Al_2O_3, the diffraction peaks (2θ = 14, 33.2, and 58.7°) corresponding to the (002), (100), and (110) planes of MoS_2 (JCPDS#75-1539) were observed. In addition, the same diffraction peaks (30.7, 32.6, and 50.2°) in the patterns of

both K-MoS_2/Al_2O_3 and K-Mo_2C/Al_2O_3 were assigned to K_2MoO_4 (JCPDS- ICDD#29-1021), indicating interactions between K and Mo.

Raman spectroscopy was used to determine the molecular structure of the samples by analyzing the vibrational and rotational modes of their chemical bonds. Figure 2c shows the Raman spectra of the K-MoS_2/Al_2O_3 and K-Mo_2C/Al_2O_3 to provide further evidence of the effects of vulcanization and carbonization treatments. K-Mo_2C/Al_2O_3 displayed an intense band near 215 cm^{-1}, which corresponded to the well-dispersed $AlMo_6O_{24}H_6{}^{3+}$ heteropolyacid anion ($AlMo_6$) formed by mixing an alumina support with a molybdenum-based aqueous solution [30]. The bands at 325 cm^{-1}, 896 cm^{-1}, and 917 cm^{-1} were attributed to K_2MoO_4 and $K_2Mo_2O_7$, which is consistent with the XRD patterns [31,32]. K-Mo_2C/Al_2O_3 catalyst also showed distinct characteristic peaks at 661 cm^{-1}, 818 cm^{-1}, and 990 cm^{-1}, which corresponded to the stretching vibrations of Mo-C-Mo and Mo-C, respectively, indicating the presence of Mo_2C [33]. For K-MoS_2/Al_2O_3, the main bands at 378 cm^{-1} and 404 cm^{-1} were assigned to the in-plane $E^1{}_{2g}$ mode resulting from the opposite vibrations of two S atoms with respect to the Mo atom. The A_{1g} mode was related to the out-of-plane vibrations of S atoms in opposite directions, respectively, further demonstrating the existence of MoS_2.

2.2.2. Redox Properties of K-Mo Catalysts

H_2-temperature programmed reduction (H_2-TPR) experiments are commonly used to investigate the properties and amounts of active sulfur species over MoS_2-based catalysts. The H_2-TPR curves of K-MoS_2/SiO_2 and K-MoS_2/Al_2O_3 catalysts are shown in Figure S1. Two reduction peaks were observed over K-MoS_2/SiO_2 and K-MoS_2/Al_2O_3 catalysts at 300–400 °C and 500–600 °C. Typically, the reduction peaks located in the low-temperature region (300–400 °C) are attributed to surface-active sulfur species on the exposed coordinatively unsaturated sites (CUS) of MoS_2 [34]. The reduction peaks in the mid-temperature region (500–600 °C) are assigned to the consumption of hydrogen during K-S bond breakage in K-containing crystalline phases [34]. As reported in the literature, the consumption of hydrogen in the low-temperature region of H_2-TPR determines the strength of the Mo-S bonds, which reflects the number of surface-active sulfur species. The H_2 consumption over K-MoS_2/Al_2O_3 was much larger than that over K-MoS_2/SiO_2, indicating that more reactive sulfur species were present on the surface of K-Mo/Al_2O_3. Furthermore, the reduction temperature over K-MoS_2/Al_2O_3 was higher than that over K-MoS_2/SiO_2, indicating stronger metal-support interactions over the K-MoS_2/Al_2O_3 catalyst [35], which promoted the dispersion of active species on the support [36]. Active sulfur species exhibit high performance during the synthesis of CH_3SH from $CO/H_2/H_2S$; therefore, K-MoS_2/Al_2O_3 is a more suitable choice, which is consistent with the activity tests in Figure 1. Notably, three distinct hydrogen consumption peaks were observed over the K-Mo_2C/Al_2O_3 catalyst at 200–350 °C, 400–600 °C, and >600 °C, respectively (Figure 3). Typically, the hydrogen consumption peaks in the low-temperature region are assigned to the reduction of the passivation layer on the surface of molybdenum carbide [37]. The reduction peak in the mid-temperature region is attributed to the reduction of Mo^{6+} to Mo^{4+} [38], and the reduction peak in the high-temperature region is attributed to the reduction of Mo^{4+} to Mo [39]. However, the sample was not passivated, so it can be assumed that there was no passivation layer on its surface. According to the previous literature, the hydrogen consumption peak at low temperatures (200–400 °C) was also attributed to the reduction of high-valent molybdenum oxides on the surface. Combined with the H_2-TPR results for K-containing molybdenum sulfide catalysts, the three hydrogen consumption peaks (200–350 °C, 400–600 °C, and >600 °C) were attributed to the reduction of Mo^{4+}, the breakage of K-C bonds in the K crystalline phase, and the reduction of Mo^{2+} (Mo_2C) to elemental Mo, respectively. Compared with the H_2-TPR curves of K-MoS_2/Al_2O_3 and K-Mo_2C/Al_2O_3, the K-MoS_2/Al_2O_3 catalyst exhibited a higher reduction temperature and greater hydrogen consumption. This indicates that K-MoS_2/Al_2O_3 displayed stronger metal-support interactions and more coordinatively unsaturated molybdenum sites (Mo-CUS) than K-Mo_2C/Al_2O_3.

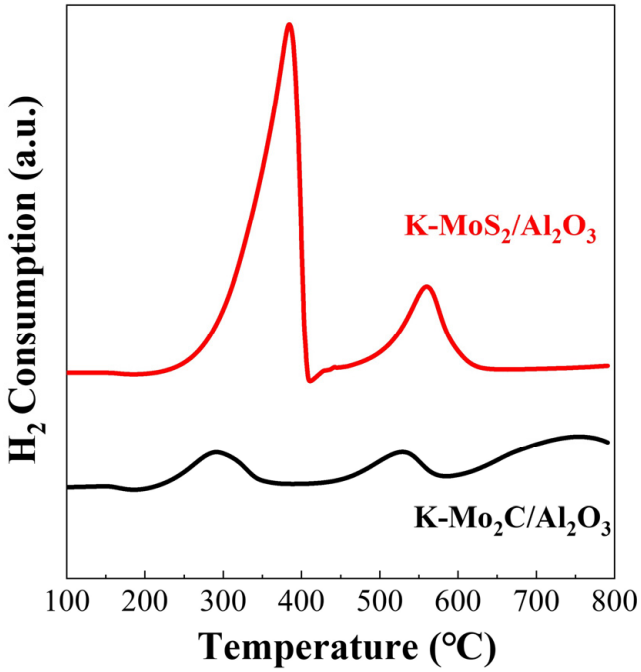

Figure 3. H_2-TPR curves of K-MoS_2/Al_2O_3 and K-Mo_2C/Al_2O_3.

2.2.3. Temperature-Programmed Desorption of Reactants ($CO/H_2/H_2S$-TPD)

Adsorption is an important stage during any catalytic reaction; thus, it is necessary to further consider the adsorption properties over catalysts for the reactants. As shown in Figure 4, $CO/H_2/H_2S$-TPD was carried out to test the chemisorption and activation of $CO/H_2/H_2S$ over K-MoS_2/Al_2O_3 and K-Mo_2C/Al_2O_3 catalysts. In Figure 4a, both K-MoS_2/Al_2O_3 and K-Mo_2C/Al_2O_3 displayed three desorption peaks of CO at 100–200 °C, 400–500 °C, and 500–700 °C. In the low-temperature region, the desorption peak of CO over K-Mo_2C/Al_2O_3 was due to the physical adsorption of CO on Mo_2C, whereas the desorption peak of CO over K-MoS_2/Al_2O_3 was attributed to the non-dissociative adsorption of CO over Mo-CUS. The peak area of K-Mo_2C/Al_2O_3 was much higher than that of K-MoS_2/Al_2O_3, indicating the larger surface area of the former. In the mid-temperature regions, the CO desorption peaks for K-Mo_2C/Al_2O_3 and K-MoS_2/Al_2O_3 were attributed to the weak chemisorption on Mo_2C and the desorption of CO from –SH groups [40], respectively. In the high-temperature region, the desorption peak of CO for K-Mo_2C/Al_2O_3 was attributed to strong chemisorption on Mo_2C, while the desorption peaks of CO for K-MoS_2/Al_2O_3 were related to the dissociative adsorption of CO with kinetic control or sulfur-containing compounds. Generally, dissociatively adsorbed CO tends to form hydrocarbon products. During the hydrogenation reaction, the adsorption and activation of H_2 molecules are important. H_2 molecules that are readily activated to adsorbed H* facilitate the formation of CH_3S* species with C-S intermediates, while the presence of gaseous H_2 facilitates the hydrolysis of C-S intermediates to form CH_x* and SH*. The latter of these is detrimental to the synthesis of CH_3SH. The H_2-TPD curves in Figure 4b show that K-Mo_2C/Al_2O_3 produced a large amount of desorbed H in the mid-temperature region, with a clear H_2 inversion peak at 700 °C, indicating that hydrogen may have dissociated into adsorbed H*. However, there was no obvious H_2 desorption peak over the K-Mo_2S/Al_2O_3 catalyst. In summary, the K-Mo_2C/Al_2O_3 catalyst showed better adsorption and activation ability for CO and H_2, and the formed H* stabilized the C-S bond and hydrogenated CH_3SH. As for H_2S-TPD in Figure 4c, almost no difference was observed between K-Mo_2C/Al_2O_3 and K-MoS_2/Al_2O_3 in the low- and high-temperature regions. A weak desorption peak of H_2S appeared over the K-Mo_2C/Al_2O_3 catalyst near 400 °C, while almost no desorption peak appeared for K-MoS_2/Al_2O_3, indicating that Mo_2C adsorbed H_2S at moderate temperatures. According to Figure 1, the optimal reaction temperature for

the synthesis of CH_3SH was in the range of about 300–400 °C, so the appropriate desorption temperature of H_2S for the K-Mo_2C/Al_2O_3 catalyst promoted the synthesis of CH_3SH.

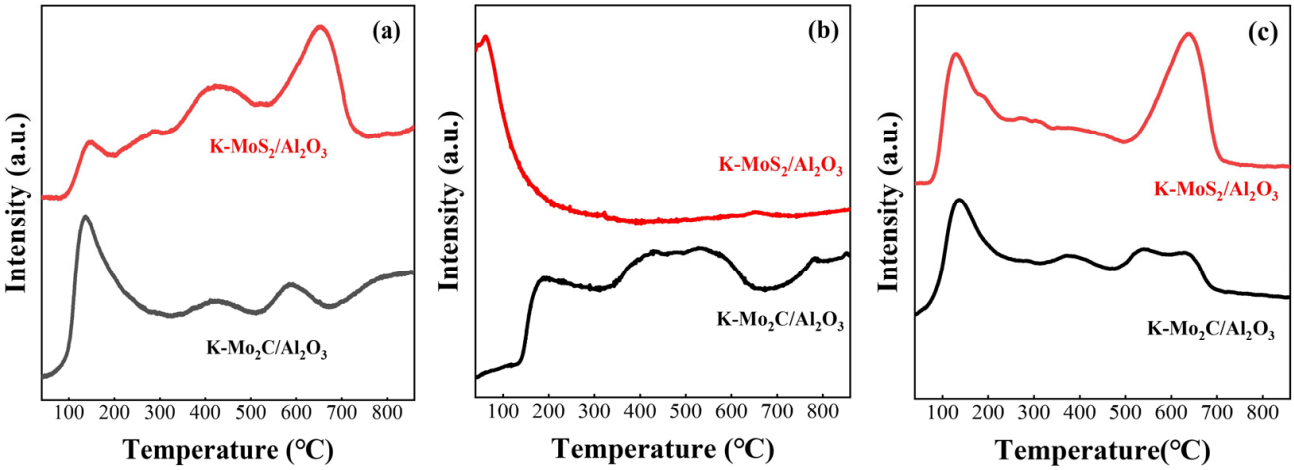

Figure 4. $CO/H_2/H_2S$-TPD (**a**–**c**) of K-MoS_2/Al_2O_3 and K-Mo_2C/Al_2O_3.

2.2.4. Catalytic Performance of Sulfided and Carbonized Catalysts

The consumption rate of CO, the formation rate of CH_3SH, and the selectivity of products over K-Mo_2C/Al_2O_3 and K-MoS_2/Al_2O_3 catalysts during the synthesis of CH_3SH from $COS/H_2/H_2S$ are presented in Figure 5. K-Mo_2C/Al_2O_3 exhibited better excellent catalytic activity in Figure 5a,b, and the rates of CO consumption and CH_3SH formation with temperature followed similar trends over both K-Mo_2C/Al_2O_3 and K-MoS_2/Al_2O_3 catalysts. The highest catalytic activity over the K-Mo_2C/Al_2O_3 catalyst was achieved at 325 °C when the consumption rate of CO reached 0.2660 $g \cdot g_{cat}^{-1} \cdot h^{-1}$, and the formation rate of CH_3SH reached 0.2990 $g \cdot g_{cat}^{-1} \cdot h^{-1}$. The consumption rate of CO over the K-MoS_2/Al_2O_3 catalyst reached a maximum of only 0.2257 $g \cdot g_{cat}^{-1} \cdot h^{-1}$ at 350 °C, and the formation rate of CH_3SH reached a maximum of only 0.1795 $g \cdot g_{cat}^{-1} \cdot h^{-1}$ at 325 °C. As shown in Figure 5c,d, there was no significant difference in the variety of products (CH_3SH, COS, CO_2, CH_4, and CS_2), and CH_3SH was the main product. K-Mo_2C/Al_2O_3 exhibited higher CH_3SH selectivity and lower COS selectivity, and no significant difference was found in the selectivity of the remaining products. These results indicate that the carbonized catalyst possessed a higher COS hydrogenation capacity.

2.3. Discussion

First, the reaction conditions for CH_3SH synthesis were optimized by regulating the pressure during the reaction and trying different supports. The pressurized conditions improved the CO conversion efficiency and CH_3SH selectivity, which was attributed to the presence of more active sulfur species on the surface of K-MoS_2/Al_2O_3 catalysts and the favorable dispersion of the active species when using Al_2O_3 as the support. In addition, the ex situ characterization of sulfided K-MoS_2/Al_2O_3 catalyst and carbonized K-Mo_2C/Al_2O_3 catalyst were combined with their activity tests during CH_3SH synthesis from $COS/H_2/H_2S$. The carbonized K-Mo_2C/Al_2O_3 catalyst exhibited higher catalytic performance than the sulfided K-MoS_2/Al_2O_3 catalyst. The XRD and Raman spectra show that the molybdenum sulfide and molybdenum carbide phases were formed in the oxidized K-Mo/Al_2O_3 samples, which differed depending on sulfurization and carbonization treatment, respectively. K-Mo oxides remained in the catalysts after pretreatment, indicating interactions between the molybdate and K. H_2-TPR showed that the sulfided K-MoS_2/Al_2O_3 catalyst exhibited higher hydrogen reduction peaks, but this was not directly related to the catalytic activity. According to $CO/H_2/H_2S$-TPD, K-Mo_2C/Al_2O_3 showed a greater activation capacity for CO and H_2 than the sulfided K-MoS_2/Al_2O_3 catalyst. The activity tests showed that the K-Mo_2C/Al_2O_3 catalysts exhibited a higher CO consumption

rate. Analysis of the product selectivity showed that the K-Mo_2C/Al_2O_3 catalyst showed superior hydrogenation capacity for COS and CS_2, which may be related to its excellent hydrogen activation capacity.

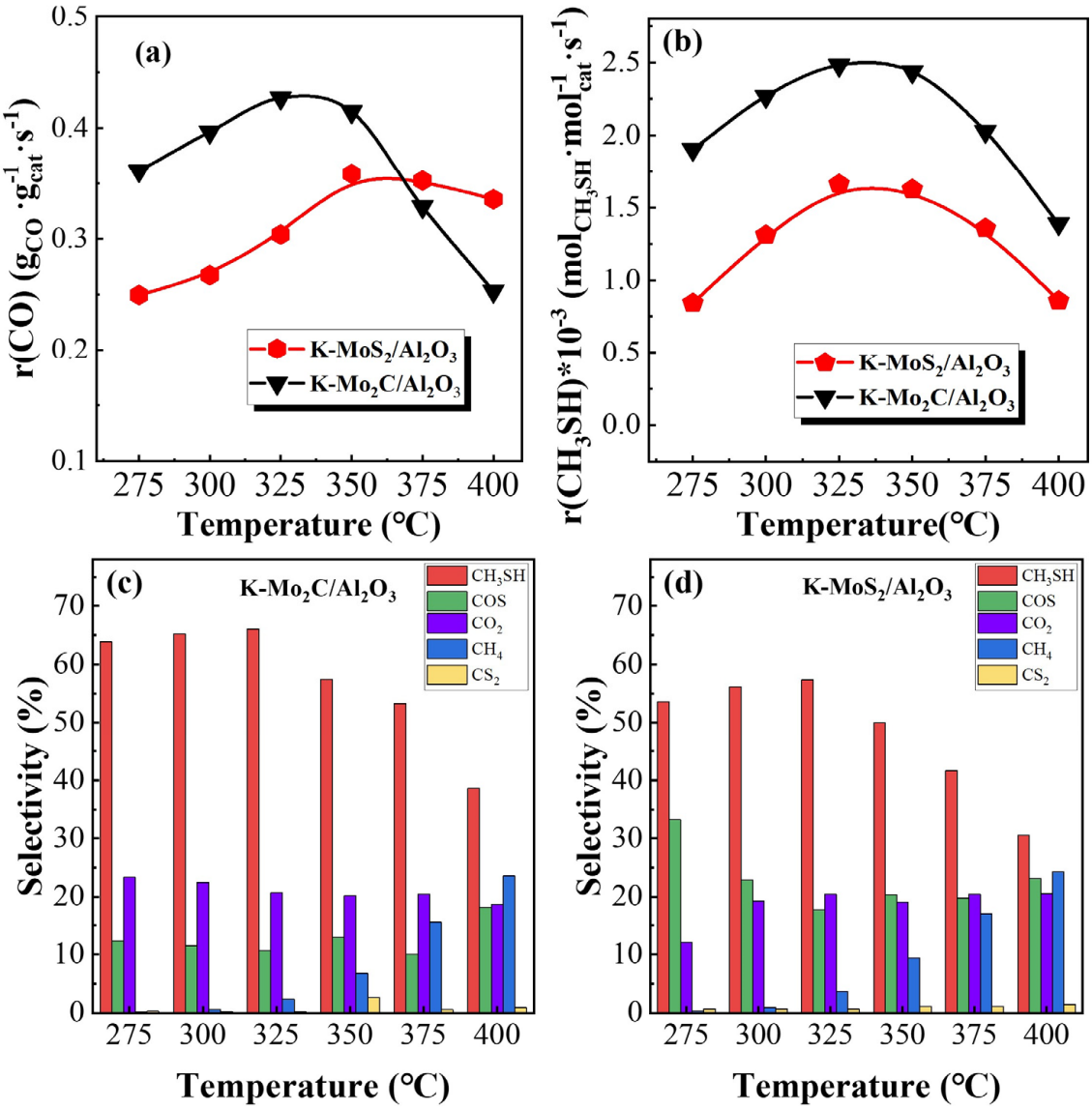

Figure 5. Consumption rate of CO (**a**) and the formation rate of CH_3SH (**b**) over K-MoS_2/Al_2O_3 and K-Mo_2C/Al_2O_3. CH_3SH selectivity over K-MoS_2/Al_2O_3 (**c**) and K-Mo_2C/Al_2O_3 (**d**).

Finally, we elucidated the corresponding catalytic reaction mechanisms for the conversion of $CO/H_2/H_2S$ to CH_3SH over carbonization-treated and sulfidation-treated K-Mo-based catalysts. The similarity was that COS was first generated by the reaction of CO and H_2S, and then CH_3CH was synthesized by direct or indirect hydrogenation of COS. Over the K-MoS_2/Al_2O_3 catalyst, the stronger metal-support interactions and the greater number of exposed unsaturated molybdenum sites favored the adsorption and activation of CO and H_2S. The production of K_2S was key to the synthesis of CH_3SH and also stabilized the C-S bonds, thus avoiding the conversion of COS to side products in the gas phase. For the K-Mo_2C/Al_2O_3 catalyst, Mo_xC facilitated the adsorption and activation of H_2, and active H atoms accelerated the hydrogenation of COS to SH_3CH, which explains why K-Mo_2C/Al_2O_3 exhibited a higher SH_3CH selectivity.

3. Experimental Section

3.1. Catalyst Preparation

γ-Al_2O_3 (purity > 99.98%) and SiO_2 (purity > 99.99%) were purchased from Chongqing Chuandong Chemical Co., Ltd., Chongqing, China; $(NH_4)_6Mo_7O_{24}\cdot 4H_2O$ (purity > 98%) was purchased from Tianjin No. 4 Chemical Reagent Factory, China; K_2CO_3 (purity > 99.99%) was purchased from Lianyungang Xinfu Rare Earth Co., Ltd., Lianyungang, China. All medicines were not further purified.

3.1.1. Preparation of K-MoO_3/Al_2O_3 and K-MoO_3/SiO_2

K-MoO_3/Al_2O_3 and K-MoO_3/SiO_2 catalysts were prepared by using the incipient-wetness co-impregnation method with γ-Al_2O_3 and SiO_2 as supports, respectively, K_2CO_3 as the K precursor, and $(NH_4)_6Mo_7O_{24}\cdot 4H_2O$ as the molybdenum precursor. Before γ-Al_2O_3 (noted as "Al_2O_3" hereafter) was used, it was calcined in a muffle furnace at 550 °C for 6 h. The loading of Mo (based on MoO_3) and the molar ratios of K:Mo were 10 wt% and 2:1, respectively. After impregnation, the samples were dried at 110 °C for 12 h and then calcined at 550 °C for 5 h in muffle furnace under still air. After cooling, the tablets were pressed and sieved through 40–60 mesh to obtain oxidized samples, noted as K-MoO_3/Al_2O_3 and K-MoO_3/SiO_2.

3.1.2. Preparation of K-MoS_2/Al_2O_3 and K-MoS_2/SiO_2

K-MoO_3/Al_2O_3 or K-MoO_3/SiO_2 samples (0.8 g; 40–60 mesh) were fixed at the center of the tube furnace reactor, and then a mixture of H_2/H_2S with a total flow rate of 40 mL/min was introduced, and the temperature of the reactor was increased to 400 °C and held for 4 h. The volume ratio of H_2: H_2S was 9:1, and the heating rate was 5 °C/min. The sulfated samples were noted as K-MoS_2/Al_2O_3 and K-MoS_2/SiO_2, respectively.

3.1.3. Preparation of K-Mo_2C/Al_2O_3

K-MoO_3/Al_2O_3 samples (0.8 g; 40–60 mesh) were fixed in the center of the tube furnace reactor. Then, a mixture of H_2/CH_4 with a total flow rate of 40 mL/min was introduced, and the temperature of the reactor was increased to 300 °C and maintained for 2 h. Then, it was increased to 500 °C for 2 h (1 °C/min), where the volume ratio of H_2:CH_4 was 9:1, and the heating rate was 5 °C/min. The carbonized sample was noted as K-Mo_2C/Al_2O_3.

3.2. Catalyst Characterization

The details of catalyst characterizations are listed in the Supplementary Materials.

3.3. Catalytic Performance Evaluation

The catalyst activity was evaluated over a 6 mm i.d. quartz fixed-bed using 0.4 g of catalyst (40–60 mesh). A gas mixture of $CO/H_2/H_2S$ = 1/4/5 at a pressure of 0.2 MPa and a flow rate of 40 mL/min was used. WHSV used for tests was 6000 $mL\cdot g^{-1}\cdot h^{-1}$. The catalytic activity was measured in the range of 275–400 °C at 25 °C intervals. Samples were collected after the target temperature was reached and stabilized for 30 min, 60 min, and 90 min followed by taking the average value. The reaction products were detected online using three GC fitted with one thermal conductivity detector (TCD), one flame ionization detector (FID), and two flame photometric detectors (FPD). The CO conversion and CH_3SH selectivity were calculated by the following equations:

$$X_{(CO)}(\%) = \frac{C_{CO,in} - C_{CO,out}}{C_{CO,in}} \times 100\%$$

$$S_{CH_3SH}(\%) = \frac{C_{CH_3SH}}{C_{CH_3SH} + C_{COS} + C_{CO_2} + C_{CH_4} + C_{CS_2}} \times 100\%$$

where $C_{CO,in}$ denotes the concentration of CO in the feed gas; $C_{CO,out}$ denotes the concentration of CO in the product; and C_{CH_3SH}, C_{COS}, C_{CO_2}, C_{CH_4}, and C_{CS_2} represent the concentration of CH_3SH, COS, CO_2, CH_4, and CS_2 in the product, respectively.

The consumption rate of CO and the formation rate of CH_3SH were calculated by the following equation:

$$r_{(CO)} = \frac{M_{co} \times C_{co,in} \times X_{(CO)} \times Q}{V_m \times m_{cat}} = \mathrm{g} \times \mathrm{g_{cat}}^{-1} \times \mathrm{s}^{-1}$$

$$r_{(CH_3SH)} = \frac{M_{CH3SH} \times Q}{V_m \times M_{cat}} = \mathrm{mol} \times \mathrm{mol_{cat}}^{-1} \times \mathrm{s}^{-1}$$

where M_{CO} is the CO molar mass (g/mol), M_{CH3SH} is the CH_3SH molar of the product (mol), Q is the flow rate, V_m is the molar volume of gas at standard conditions (L/mol), and M_{cat} is the molar of catalyst used (mol).

4. Conclusions

In this work, we compared the catalytic performance of K-Mo_2S catalysts with different supports. Based on the H_2-TPR results, the metal-support interactions over the K-MoS_2/Al_2O_3 catalyst were much stronger than those over the K-MoS_2/SiO_2 catalyst, which improved the dispersion of active species on the support surface. The exposure of more Mo-CUS over the K-MoS_2/Al_2O_3 catalyst accelerated the reaction. Moreover, the K-Mo_2C/Al_2O_3 catalyst obtained by the carbonization of oxidized K-Mo-based catalysts also showed excellent catalytic performance for the conversion of $CO/H_2/H_2S$ to CH_3SH. K-Mo_2C/Al_2O_3 exhibited a higher CO consumption rate and CH_3SH selectivity than K-MoS_2/Al_2O_3. More importantly, the $CO/H_2/H_2S$-TPD experiments and characterization results confirmed that the strong metal-support interactions and the formation of K_2S over the K-MoS_2/Al_2O_3 catalyst favored the adsorption and activation of CO/H_2S. The K-Mo_2C/Al_2O_3 catalyst showed a superior ability to activate H_2. In contrast, the activation of hydrogen was more favorable for the hydrogenation of the intermediate species COS to CH_3SH, thus improving the selectivity of CH_3SH in the products.

Supplementary Materials: The following supporting information can be downloaded at: https://www.mdpi.com/article/10.3390/catal14030190/s1, Figure S1: H2-TPR curves of K-MoS_2/SiO_2 and K-MoS_2/Al_2O_3.

Author Contributions: Conceptualization, D.Z. and M.L.; data curation, H.W., W.Z., J.F., M.L. and Y.L. (Yongming Luo); formal analysis, J.F. and M.L.; funding acquisition, Y.L. (Yongming Luo); investigation, H.W., W.Z., Y.L. (Yubei Li) and J.F.; methodology, Y.L. (Yubei Li); project administration, D.Z., J.L. and Y.L. (Yongming Luo); resources, D.Z., J.L. and Y.L. (Yongming Luo); supervision, W.Z. and J.L.; validation, Y.L. (Yubei Li) and J.F.; writing—original draft, H.W., Y.L. (Yubei Li) and M.L.; writing—review and editing, H.W., W.Z., D.Z., J.L. and Y.L. (Yongming Luo). All authors have read and agreed to the published version of the manuscript.

Funding: We are grateful for the financial support from the National Natural Science Foundation of China (Grant No. 42030712, 22106055, and 21966018), the Yunnan Major Scientific and Technological Projects (Grant No. 202302AG050002/KKAU202322028), the Key Project of the Natural Science Foundation of Yunnan Province (Grant No. 202101AS070026), and the Applied Basic Research Foundation of Yunnan Province (Grant No. 202301AW070019, 202201AT070086, 202101AU070025, 202101BE07000-1026 and 202105AE160019), as well as the Yunnan Ten Thousand Talents Plan Young & Elite Talents Project (No. YNWR-QNBJ-2018-067).

Data Availability Statement: Data are available in the manuscript.

Conflicts of Interest: The authors declare no conflict of interest.

References

1. Lu, J.; Liu, P.; Xu, Z.; He, S.; Luo, Y. Investigation of the reaction pathway for synthesizing methyl mercaptan (CH_3SH) from H_2S-containing syngas over K-Mo-type materials. *RSC Adv.* **2018**, *8*, 21340–21353. [CrossRef]
2. Lu, J.C.; Luo, Y.M.; He, D.D.; Xu, Z.Z.; He, S.F.; Xie, D.L.; Mei, Y. An exploration into potassium (K) containing MoS_2 active phases and its transformation process over MoS_2 based materials for producing methanethiol. *Catal. Today* **2020**, *339*, 93–104. [CrossRef]
3. Pérez, H.A.; López, C.A.; Cadús, L.E.; Agüero, F.N. Catalytic feasibility of Ce-doped $LaCoO_3$ systems for chlorobenzene oxidation: An analysis of synthesis method. *J. Rare Earths* **2022**, *40*, 897–905. [CrossRef]
4. Clark, P.D.; Dowling, N.I.; Huang, M. Conversion of CS_2 and COS over alumina and titania under Claus process conditions: Reaction with H_2O and SO_2. *Appl. Catal. B Environ.* **2001**, *31*, 107–112. [CrossRef]
5. Yao, X.-Q.; Li, Y.-W. Density functional theory study on the hydrodesulfurization reactions of COS and CS_2 with Mo_3S_9 model catalyst. *J. Mol. Struct.* **2009**, *899*, 32–41. [CrossRef]
6. Park, N.-K.; Han, D.C.; Lee, T.J.; Ryu, S.O. A study on the reactivity of Ce-based Claus catalysts and the mechanism of its catalysis for removal of H_2S contained in coal gas. *Fuel* **2011**, *90*, 288–293. [CrossRef]
7. Yao, S.Y.; Mudiyanselage, K.; Xu, W.Q.; Johnston-Peck, A.C.; Hanson, J.C.; Wu, T.P.; Stacchiola, D.; Rodriguez, J.A.; Zhao, H.Y.; Beyer, K.A.; et al. Unraveling the Dynamic Nature of a CuO/CeO_2 Catalyst for CO Oxidation in Operando: A Combined Study of XANES (Fluorescence) and DRIFTS. *ACS Catal.* **2014**, *4*, 1650–1661. [CrossRef]
8. Xie, Y.; Wu, J.F.; Jing, G.J.; Zhang, H.; Zeng, S.H.; Tan, X.P.; Zou, X.Y.; Wen, J.; Su, H.Q.; Zhong, C.J.; et al. Structural origin of high catalytic activity for preferential CO oxidation over CuO/CeO_2 nanocatalysts with different shapes. *Appl. Catal. B Environ.* **2018**, *239*, 665–676. [CrossRef]
9. Gutiérrez, O.Y.; Kaufmann, C.; Lercher, J.A. Influence of Potassium on the Synthesis of Methanethiol from Carbonyl Sulfide on Sulfided Mo/Al_2O_3 Catalyst. *ChemCatChem* **2011**, *3*, 1480–1490. [CrossRef]
10. Gutiérrez, O.Y.; Kaufmann, C.; Hrabar, A.; Zhu, Y.; Lercher, J.A. Synthesis of methyl mercaptan from carbonyl sulfide over sulfide K_2MoO_4/SiO_2. *J. Catal.* **2011**, *280*, 264–273. [CrossRef]
11. Lamonier, C.; Lamonier, J.-F.; Aellach, B.; Ezzamarty, A.; Leglise, J. Specific tuning of acid/base sites in apatite materials to enhance their methanol thiolation catalytic performances. *Catal. Today* **2011**, *164*, 124–130. [CrossRef]
12. Pashigreva, A.V.; Kondratieva, E.; Bermejo-Deval, R.; Gutiérrez, O.Y.; Lercher, J.A. Methanol thiolation over Al_2O_3 and WS_2 catalysts modified with cesium. *J. Catal.* **2017**, *345*, 308–318. [CrossRef]
13. Lu, J.; Li, X.; He, S.; Han, C.; Wan, G.; Lei, Y.; Chen, R.; Liu, P.; Chen, K.; Zhang, L.; et al. Hydrogen production via methanol steam reforming over Ni-based catalysts: Influences of Lanthanum (La) addition and supports. *Int. J. Hydrog. Energy* **2017**, *42*, 3647–3657. [CrossRef]
14. Gutiérrez, O.Y.; Klimova, T. Effect of the support on the high activity of the (Ni)Mo/ZrO_2–SBA-15 catalyst in the simultaneous hydrodesulfurization of DBT and 4,6-DMDBT. *J. Catal.* **2011**, *281*, 50–62. [CrossRef]
15. Enyashin, A.N.; Yadgarov, L.; Houben, L.; Popov, I.; Weidenbach, M.; Tenne, R.; Bar-Sadan, M.; Seifert, G. New Route for Stabilization of 1T-WS_2 and MoS_2 Phases. *J. Phys. Chem. C* **2011**, *115*, 24586–24591. [CrossRef]
16. Andersen, A.; Kathmann, S.M.; Lilga, M.A.; Albrecht, K.O.; Hallen, R.T.; Mei, D. First-Principles Characterization of Potassium Intercalation in Hexagonal 2H-MoS_2. *J. Phys. Chem. C* **2012**, *116*, 1826–1832. [CrossRef]
17. Gutiérrez, O.Y.; Zhong, L.; Zhu, Y.; Lercher, J.A. Synthesis of Methanethiol from CS_2 on Ni-, Co-, and K-Doped MoS_2/SiO_2Catalysts. *ChemCatChem* **2013**, *5*, 3249–3259. [CrossRef]
18. Lu, J.C.; Fang, J.; Xu, Z.Z.; He, D.D.; Feng, S.Y.; Li, Y.B.; Wan, G.P.; He, S.F.; Wu, H.; Luo, Y.M. Facile synthesis of few-layer and ordered K-promoted MoS_2 nanosheets supported on SBA-15 and their potential application for heterogeneous catalysis. *J. Catal.* **2020**, *385*, 107–119. [CrossRef]
19. Liu, P.; Lu, J.; Xu, Z.; Liu, F.; Chen, D.; Yu, J.; Liu, J.; He, S.; Wan, G.; Luo, Y. The effect of alkali metals on the synthesis of methanethiol from $CO/H_2/H_2S$ mixtures on the SBA-15 supported Mo-based catalysts. *Mol. Catal.* **2017**, *442*, 39–48. [CrossRef]
20. Fang, J.; Lu, J.C.; Xu, Z.Z.; Feng, S.Y.; Li, Y.B.; He, B.H.; Luo, M.; Wang, H.; Luo, Y.M. Modulation the metal-support interactions of potassium molybdenum-based catalysts for tuned catalytic performance of synthesizing CH_3SH. *Sep. Purif. Technol.* **2023**, *316*, 123815. [CrossRef]
21. El-Bahy, Z.M.; Alotaibi, M.T.; El-Bahy, S.M. CO oxidation and 4-nitrophenol reduction over ceria-promoted platinum nanoparticles impregnated with ZSM-5 zeolite. *J. Rare Earths* **2022**, *40*, 1247–1254. [CrossRef]
22. Zhang, Q.; Zhou, Z.; Fang, T.; Gu, H.; Guo, Y.; Zhan, W.; Guo, Y.; Wang, L. Understanding the role of tungsten on Pt/CeO_2 for vinyl chloride catalytic combustion. *J. Rare Earths* **2022**, *40*, 1462–1470. [CrossRef]
23. Marquart, W.; Raseale, S.; Prieto, G.; Zimina, A.; Sarma, B.B.; Grunwaldt, J.D.; Claeys, M.; Fischer, N. CO_2 Reduction over Mo_2C-Based Catalysts. *ACS Catal.* **2021**, *11*, 1624–1639. [CrossRef]
24. Zhou, H.; Chen, Z.; Kountoupi, E.; Tsoukalou, A.; Abdala, P.M.; Florian, P.; Fedorov, A.; Müller, C.R. Two-dimensional molybdenum carbide 2D-Mo_2C as a superior catalyst for CO_2 hydrogenation. *Nat. Commun.* **2021**, *12*, 5510. [CrossRef]
25. Xiong, K.; Zhou, G.; Zhang, H.; Shen, Y.; Zhang, X.; Zhang, Y.; Li, J. Bridging Mo_2C-C and highly dispersed copper by incorporating N-functional groups to greatly enhance the catalytic activity and durability for carbon dioxide hydrogenation. *J. Mater. Chem. A* **2018**, *6*, 15510–15516. [CrossRef]
26. Calais, J.-L. Band structure of transition metal compounds. *Adv. Phys.* **1977**, *26*, 847–885. [CrossRef]

27. Duan, D.; Hao, C.; He, G.; Wen, Y.; Sun, Z. Rh/CeO_2 composites prepared by combining dealloying with calcination as an efficient catalyst for CO oxidation and CH_4 combustion. *J. Rare Earths* **2022**, *40*, 636–644. [CrossRef]
28. Ma, Y.; Li, Z.; Zhao, N.; Teng, Y. One-pot synthesis of Cu–Ce co-doped SAPO-5/34 hybrid crystal structure catalysts for NH_3-SCR reaction with SO_2 resistance. *J. Rare Earths* **2021**, *39*, 1217–1223. [CrossRef]
29. Liu, W.; Cao, H.; Wang, Z.; Cui, C.; Gan, L.; Liu, W.; Wang, L. A novel ceria hollow nanosphere catalyst for low temperature NO_x storage. *J. Rare Earths* **2022**, *40*, 626–635. [CrossRef]
30. Carrier, X.; Lambert, J.F.; Che, M. Ligand-Promoted Alumina Dissolution in the Preparation of MoO_X/γ-Al_2O_3 Catalysts: Evidence for the Formation and Deposition of an Anderson-type Alumino Heteropolymolybdate. *J. Am. Chem. Soc* **1997**, *119*, 10137–10146. [CrossRef]
31. Pérez-Martínez, D.J.; Eloy, P.; Gaigneaux, E.M.; Giraldo, S.A.; Centeno, A. Study of the selectivity in FCC naphtha hydrotreating by modifying the acid–base balance of CoMo/γ-Al_2O_3 catalysts. *Appl. Catal. A Gen.* **2010**, *390*, 59–70. [CrossRef]
32. Hao, Y.; Zhang, Y.; Chen, A.; Fang, W.; Yang, Y. Study on Methanethiol Synthesis from H_2S-Rich Syngas Over K_2MoO_4 Catalyst Supported on Electrolessly Ni-Plated SiO_2. *Catal Lett.* **2009**, *129*, 486–492. [CrossRef]
33. Hussain, S.; Zaidi, S.A.; Vikraman, D.; Kim, H.-S.; Jung, J. Facile preparation of molybdenum carbide (Mo_2C) nanoparticles and its effective utilization in electrochemical sensing of folic acid via imprinting. *Biosens. Bioelectron.* **2019**, *140*, 111330. [CrossRef]
34. Pinilla, J.L.; Purón, H.; Torres, D.; de Llobet, S.; Moliner, R.; Suelves, I.; Millan, M. Carbon nanofibres coated with Ni decorated MoS_2 nanosheets as catalyst for vacuum residue hydroprocessing. *Appl. Catal. B Environ.* **2014**, *148–149*, 357–365. [CrossRef]
35. Shi, Y.; Guo, X.; Shi, Z.; Zhou, R. Transition metal doping effect and high catalytic activity of CeO_2–TiO_2 for chlorinated VOCs degradation. *J. Rare Earths* **2022**, *40*, 745–752. [CrossRef]
36. Chang, S.; Jia, Y.; Zeng, Y.; Qian, F.; Guo, L.; Wu, S.; Lu, J.; Han, Y. Effect of interaction between different CeO_2 plane and platinum nanoparticles on catalytic activity of Pt/CeO_2 in toluene oxidation. *J. Rare Earths* **2022**, *40*, 1743–1750. [CrossRef]
37. Pang, M.; Wang, X.; Xia, W.; Muhler, M.; Liang, C. Mo(VI)–Melamine Hybrid As Single-Source Precursor to Pure-Phase β-Mo_2C for the Selective Hydrogenation of Naphthalene to Tetralin. *Ind. Eng. Chem. Res.* **2013**, *52*, 4564–4571. [CrossRef]
38. Malaibari, Z.O.; Croiset, E.; Amin, A.; Epling, W. Effect of interactions between Ni and Mo on catalytic properties of a bimetallic Ni-Mo/Al_2O_3 propane reforming catalyst. *Appl. Catal. A Gen.* **2015**, *490*, 80–92. [CrossRef]
39. Wang, G.; Schaidle, J.A.; Katz, M.B.; Li, Y.; Pan, X.; Thompson, L.T. Alumina supported Pt-Mo_2C catalysts for the water–gas shift reaction. *J. Catal.* **2013**, *304*, 92–99. [CrossRef]
40. Chen, A.; Wang, Q.; Li, Q.; Hao, Y.; Fang, W.; Yang, Y. Direct synthesis of methanethiol from H_2S-rich syngas over sulfided Mo-based catalysts. *J. Mol. Catal. A Chem.* **2008**, *283*, 69–76. [CrossRef]